Hydrothermal synthesis of ultrathin WS$_2$ nanosheets as anodes for sodium-ion batteries

X. H. Zhang[a], C. K. Yan[b,*], H. B. Cao[c], H. Tan[a], Z. Wang[d]
[a]*School of Mechanical Engineering, Jiangsu University of Technology, Changzhou 213001, Jiangsu Province, China*
[b]*Jiangsu Laboratory of Lake Environment Remote Sensing Technologies，Huaiyin Institute of Technology, HuaiAn, 223003, Jiangsu Province, China.*
[c]*School of Computer Engineering, Jiangsu University of Technology, Changzhou 213001, Jiangsu Province, China*
[d]*School of Materials and Engineering, Jiangsu University of Technology, Changzhou 213001, Jiangsu Province, China*

In this study, ultrathin WS$_2$ nanosheets with an average thickness of about 10 nm were successfully synthesized via a facile hydrothermal method. Their electrochemical properties were systematically investigated by various electrochemical testing techniques, and the morphology and structure were investigated by X-ray diffraction (XRD), scanning electron microscopy (SEM) and transmission electron microscopy (TEM). When applied as anode for sodium ion batteries, ultrathin WS$_2$ nanosheets exhibit an impressive high-rate capability and good cyclic stability, a reversible capacity of 250 mAh g^{-1} after the following cycling test of 100 cycles is still achieved at 100 mA g^{-1}. The excellent rate performance and cycling stability are attributed to better electronic conductivity and well-developed layered structure.

1. Introduction

With the widespread use of portable electronics, wearable electronics and electric vehicles, the development of renewable energy and high-efficiency energy storage devices has received extensive attention [1-5]. Among them, rechargeable batteries have become a hot research topic due to their advantages of high energy density, light weight, and fast charge and discharge rate [6-7]. Although lithium-ion batteries (LIBs) are the main rechargeable batteries for scientific research and commercial development, relatively high cost and limited lithium sources are major bottlenecks for further large-area applications [8-9]. Therefore, sodium ion batteries (SIBs) as a realistic promising alternative to LIBs are receiving increasing attention due to the abundant sodium sources and the similar chemical properties of sodium and lithium [10-12]. Despite having similar electrochemical behaviors and mechanisms to LIBs, SIBs still face great challenges in terms of cycling stability and low-rate performance. Since the radius of sodium ions (1.02 Å) is 40% larger than that of lithium ions (0.76 Å), this will produce a larger volume expansion during discharge and charge processes,

---

resulting in terrible cycle stability and rate performance [13-16]. Therefore, the development of suitable anode materials with excellent capacity and nanostructure is crucial for realizing high-performance SIBs in the future.

In recent years, ultrathin two-dimensional (2D) nanomaterials have attracted much attention due to their special layered structure, the high percentage of surface atoms and highly efficient active sites on the exposed surfaces [17-18]. The unique structure and surface properties give them an ideal morphological foundation for surface-dependent electrochemical reactions. Meanwhile, numerous studies have demonstrated that 2D nanosheets, especially those with thickness < 5 nm and lateral dimensions ranging from submicron to micrometer, possess exotic electronic properties and high specific surface area, which are very suitable for sensing, catalysis, and storage energy material [19-22]. Graphene is the most well-known 2D nanosheet while transition metal chalcogenides also play important roles as electrode materials for SIBs.

As a layered transition metal dichalcogenide, WS_2 is generally regarded as a promising anode candidate for SIBs due to its relatively larger theoretical specific capacity (432 mAh g^{-1}) than that of a commercial graphite anode. Furthermore, it possesses a large interlayer spacing of 0.62 nm and weak van der Waals interactions, which facilitates Na^+ intercalation and small volume expansion during the sodiation process [10,12,23-25]. Over the past decades, WS_2 nanoparticles with various morphologies have been synthesized and they have demonstrated a stable cyclability [23-28]. However, the electrochemical performance of ultrathin WS_2 nanosheets has rarely been investigated.

In this study, ultrathin WS_2 nanosheets were prepared by a facile hydrothermal reaction method using sodium tungstate, thiourea, oxalic acid and F127 as starting materials. The electrochemical performance of WS_2 nanosheets were investigated by a variety of electrochemical testing techniques.

2. Experimental

2.1. Synthesis of Ultrathin WS_2 Nanosheets

The raw materials, thiourea (CH_4N_2S), sodium tungstate ($Na_2WO_4 \cdot 2H_2O$), oxalic acid ($H_2C_2O_4$) and F127, were purchased from Aladdin Chemical Reagent Company. All reagents were of analytical grade and were used without further purification. In the typical synthesis, 0.99 g of sodium tungstate and 1.14 g of thiourea were first dissolved in 30mL of deionized water by magnetic stirring for 15 min. Then 0.5 grams of oxalic acid and 0.2g F127 were added to the above solution and continue stirring for 15 minutes to form a uniform suspension. The mixture solution was then transferred into a 50 ml stainless steel autoclave, sealed and heated at 240℃for 24 h. After naturally cooling to room temperature, the final black product was collected by centrifuged and washed three times with deionized water and ethanol each, and dried in an oven at 60 ℃for 12 hours.

2.2. Characterization of Ultrathin WS_2 Nanosheets

The crystal structure of the sample was analyzed by X-ray diffraction (XRD) on a powder X-ray diffraction (PW1830, Philips) with Cu Ka radiation ($\lambda = 0.1546$ nm). The 2θ range used in the measurement was from 10° to 80° with a scanning rate of 5° /min. The morphologies of the samples were recorded by a JSM-6390 (JEOL, Japan) scanning electron microscopy (SEM) equipped with

an energy-dispersive X-ray spectroscope (EDS). The transmission electron microscopy (TEM) measurement was performed on a JEM-2010 (JEOL, Japan).   The EDS was recorded coupled with SEM observation.

2.3. Electrochemical measurement

The electrochemical measurements were performed using two-electrode test cells. The working electrode was prepared by following slurry coating processing: First, 80 wt% active material, 10 wt% Super P carbon black and 10 wt% polyvinylidene fluoride were mixed N-methylpyrrolidone; then the mixed slurry was coated on a pure Cu foil; at last, the coated Cu foil was dried in vacuum at 80 °C overnight to form the working electrode. The test cells were coin cells (CR2032) which were assembled in an Ar-filled glove box, using a sodium metal foil as the counter and reference electrode, 1 M $NaClO_4$ in ethylene carbonate–diethyl carbonate (DEC)–fluoroethylene carbonate (1:1:0.02 in volume) and a glass fiber were used as the electrolyte and separator, respectively. The charge/discharge measurements were performed using a NEWWARE battery tester between 0.01~ 3 V at the current density of 100 mA g^{-1}. The cyclic voltammetry (CV) measurements were carried out using an electrochemical workstation (CHI 760D, Chenhua, Shanghai) at a scan rate of 0.1 mV s^{-1}.

3. Results and discussion

3.1. Structural and Morphological Characterization of Ultrathin WS2 Nanosheets

The powder X-ray diffraction measurement was used to characterize the crystalline structure and crystallization quality of samples. Fig. 1a shows the XRD diffraction pattern of the synthesized ultrathin WS_2 nanosheets, and all the peaks can be indexed to hexagonal phase of WS_2 (JCPDF Card No. 08-0237). The main reflection peaks located at 14.16°, 28.44°, 33.34°,36.42°, 58.94°, and 69.34° can be assigned to the (002), (004), (100), (102), (110) and (201) planes of WS_2. Moreover, the XRD signals of the sample are relatively weak amidst some background noise [29]. The reason can be attributed to the limited crystallinity of WS2. Fig. 1b illustrates the EDS spectrum of the sample, which reveals that the sample consisted of element W and S. The atomic ratio of W to S is approximately 1: 1.92, which is close to the stoichiometry of WS_2.
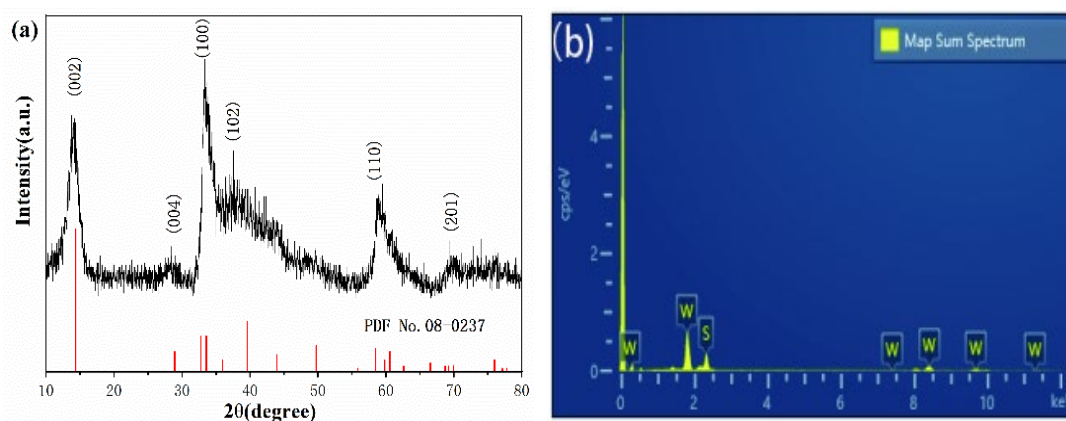
Fig. 1. (a) XRD pattern and (b) EDS of the as-prepared WS$_2$ nanosheets.

Fig. 2 shows the SEM image and elemental maps of the WS_2 samples. Fig. 2a, the low magnification SEM image, demonstrates that the sample is made up of a number of wrinkled and overlapped nanosheets. Fig. 2b presents the morphology of the WS_2 nanosheets more clearly. From which, it can be seen that the lateral size of the nanosheets is in the range of 0.5–2 μm and the thickness is about 10 nm. Moreover, the edges of the nanosheets are clearly curled. That's because the ultrathin nanosheets are unstable and it tends to roll up to form a closed structure to reduce the number of dangling bonds and the total energy of the system.[30] Fig. 2c is the EDX elemental maps of the WS_2 nanosheets, which illustrates the distribution of S, and W throughout the nanosheets.
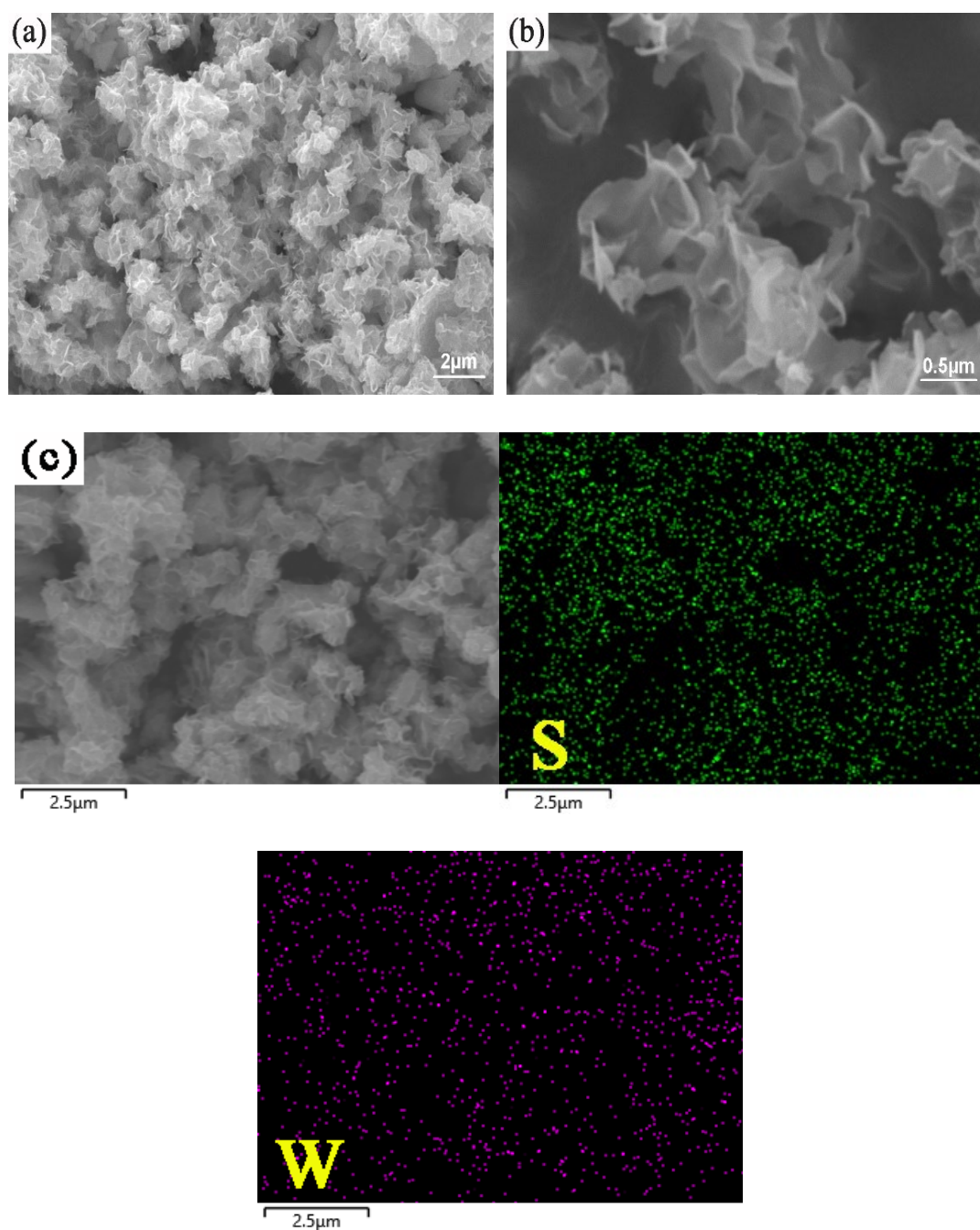
Fig. 2. FESEM (a,b) and elemental maps (c) images of the WS_2 nanosheets.

Fig. 3 shows the TEM images of the WS_2 samples. Figure 3a, the low magnification TEM image, confirms that the sample consists of ultrathin WS_2 nanosheets. In addition, it is also observed that a fraction of WS_2 nanosheets are curved. The high-resolution TEM image (Fig. 3b) shows a clear layered structure with a layer spacing of 0.65 nm, which is slightly larger than that of the (002) plane of bulk WS_2.
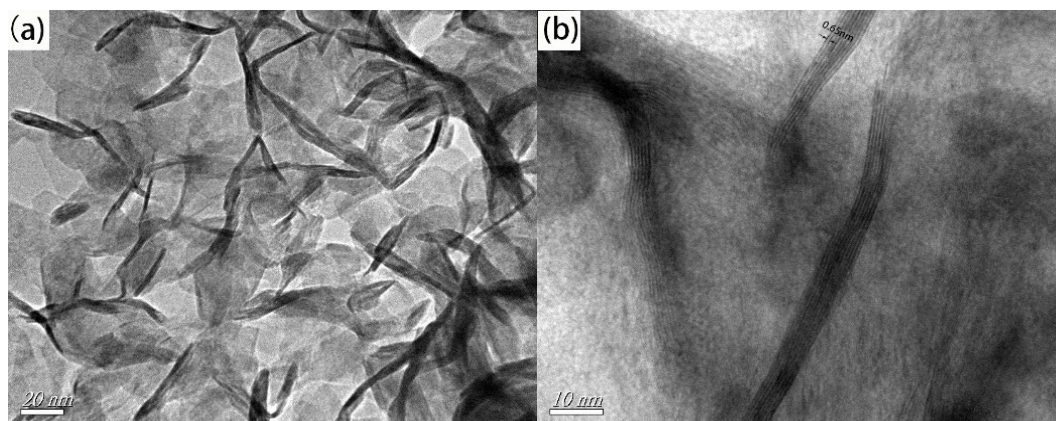
Fig. 3. TEM images of the WS_2 nanosheets.

3.2. Electrochemical Performance

The electrochemical performance of WS_2 nanosheets as SIB anode material was investigated by cyclic voltammetry (CV) tests and galvanostatic charge-discharge measurements at different densities. Fig. 4a presents the CV curves over the voltage range of 0.01-3.00 V for the first three cycles and reveals the electrochemical reactions that take place during the charge/discharge process. In the first cathodic sweep, there are three main reduction peaks presented at 0.08, 0.54 and 0.75 V. The reduction peak observed at 0.75 V could be attributed to Na^+ insertion into the layers of WS_2 to form Na_xWS_2. The two peaks at 0.08 and 0.54 V are attributed the conversion reaction of WS_2 with sodium ions into W metallic nanoparticles embedded into amorphous Na_2S matrix and the formation of the solid electrolyte interface (SEI) layer owing to the decomposition of the electrolyte. And the Na^+ storage mechanisms with WS_2 in a Na-ion battery can be described by the following equations: [10-12]

$$4Na^+ + WS_2 + 4e^- \leftrightarrow W + 2Na_2S$$

The reduction peaks in the first cycle are replaced by new weak broad peaks in the potential range from 1.2 to 2.1 V, which could be ascribed to the multistep conversion of S with Na^+ to the formation of Na_xWS_2 and Na_2S [24,25].

In the anodic sweep, there were three peaks occurring at 1.61, 1.83 and 2.15 V. According to the CV curves, the peaks at 1.83 V can be ascribed to the Na^+ extract from the Na_2S matrix [28]. The peak located at 1.61 and 2.17 V may be attributed to the oxidation of W to WS_2 [26]. The following three CV curves are almost overlapped without any shift in the redox couple positions, illustrating the superior stability of the materials.

Fig. 4b shows the galvanostatic charging/discharging profiles of the WS_2 anode material for the first three cycles at a current density of 100 mA g^{-1} in the potential range of 0.01-3 V. In the first discharge curve, there was a long plateau located at about 1.0–0.3 V which can be ascribed to sodium ions intercalation into the WS_2 lattice, WS_2 converted into W nanoparticles and the formation of SEI layer [27]. In the first charging curve, a major plateau appears around 1.8 V, which should correspond to the desodation and oxidation of W [25]. These sodiation and desodiation behaviors are consistent with the CV curves shown in Fig. 4a. The first discharge capacity is 590.8 mAh g^{-1}, while the first charge capacity is 448.2 mAh•g^{-1}. The Coulombic efficiency is 75.9% and the irreversible capacity of 142.6 mAh g^{-1} in the first cycle may be caused by the decomposition of the electrolyte and formation of the solid electrolyte interface, which is common in transition metal sulfide anodes. The curves of the third charge/discharge cycle are almost identical to those of the second, indicating good cycling reversibility and stability.
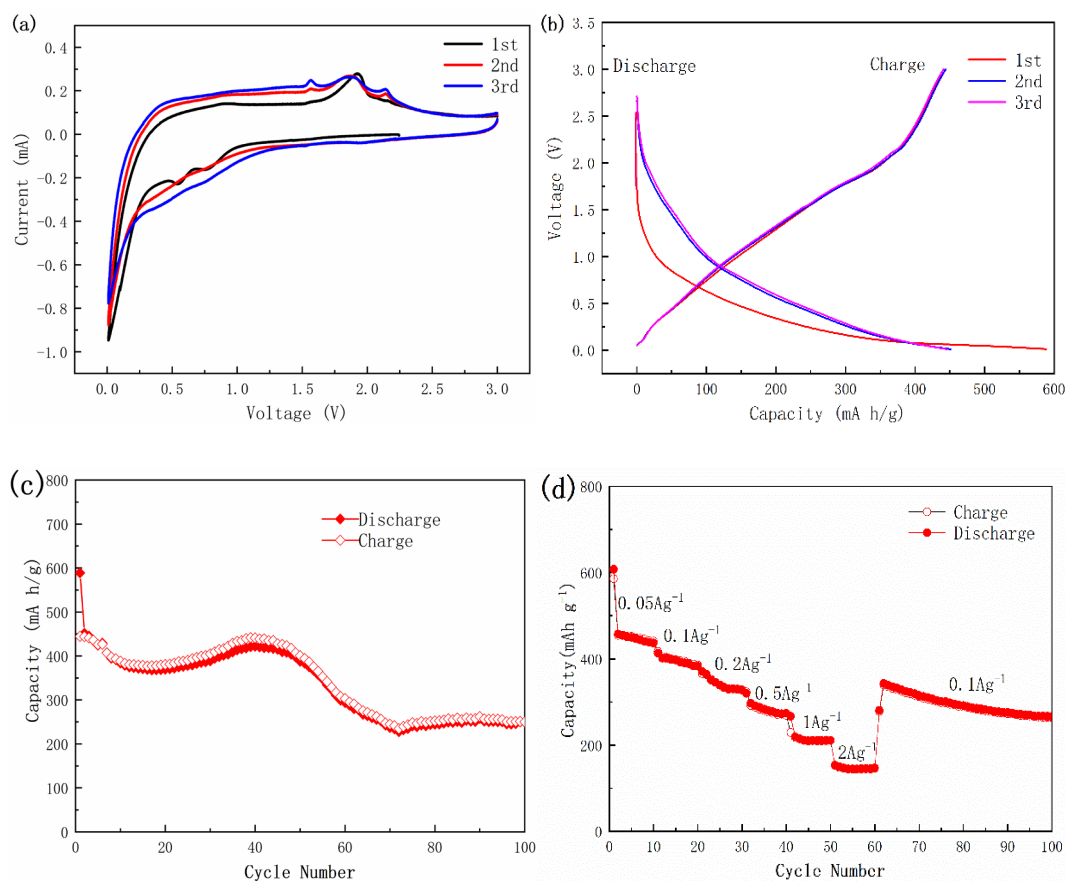
Fig. 4. (a) Cyclic voltammetry curves, (b) galvanostatic charge/discharge profiles, (c) cycle performance and (d) rate performance of WS_2 nanoflake electrode materials for SIBs.

The cycling performance of the sample is shown in Fig. 4(c). The samples exhibited better specific capacity during the first 50 cycles. After that, the specific capacity stability of the sample is not very good. Since the size of sodium ions is much larger than that of lithium ions, the volume changes during the sodiation and desodiation processes will not be well accommodated compared to

lithiation and delithiation processes. But after 100 cycles, the sodium storage capacity of the samples still remains at 250.2 mAh g^{-1}.

Fig. 4d demonstrates the rate capability of ultrathin WS$_2$ nanosheets with current densities ranging from 0.05 to 2 A g^{-1} and back to 0.1 A g^{-1}. The average discharge capacities at various current densities of 0.1, 0.2, 0.5, 1 and 2 A g^{-1} are 390, 340, 280, 210 and 145 mAh g^{-1}, respectively. As the current density recovers to 0.1 A g^{-1}, the capacity returns to about 280 mAh g^{-1}, exhibiting excellent rate performance. But the sample capacity shows rapid decay, especially at high current densities.

4. Conclusion

In conclusion, ultrathin WS$_2$ nanosheets were were synthesized by a hydrothermal reaction. When used as anode material in NIBs, ultrathin WS$_2$ nanosheets exhibit excellent electrochemical performance, maintaining a charge-discharge capacity of 250.2 mAh g^{-1} after 100 cycles at a current density of 100 mA g^{-1}. These results offer promise for the potential application of layered transition-metal disulfides as anode materials of sodium-ion batteries.

Acknowledgements

References

[1] P. Poizot, S. Laruelle, S. Grugeon, L. Dupont and J. M. Tarascon, Nature 407, 496 (2000); https://doi.org/10.1038/35035045
[2] D. Larcher and J. Tarascon, Nat. Chem. 7, 19 (2015); https://doi.org/10.1038/nchem.2085
[3] Y. Wang, B. Chen, D. H. Seo, Z. J. Han, J. I. Wong, K. K. Ostrikov, H. Zhang and H. Y. Yang, NPG Asia Mater. 8, e268 (2016); https://doi.org/10.1038/am.2016.44
[4] H. C. Chen, S. Chen, M. Q. Fan, C. Li, D. Chen, G. L. Tian and K. Y. Shu, J. Mater. Chem. A 47, 23653 (2015); https://doi.org/10.1039/C5TA08366D
[5] L. Y. Niu, Y. D. Wang, F. P. Ruan, C. Shen, S. Shan, M. Xu, Z. K. Sun, C. Li, X. J. Liu and Y. Y. Gong, J. Mater. Chem. A 4, 5669 (2016); https://doi.org/10.1039/C6TA00078A
[6] Y. Yoon, C. Park, J. Kim, D. Shin, J. Power Sources 226, 186 (2013); https://doi.org/10.1016/j.jpowsour.2012.10.094
[7] M.Y. Gao, Z.H. Tang, M.R. Wu, J.L. Chen, Y.C. Xue, X.M. Guo, Y.J. Liu, Q.H. Kong, J.H. Zhang, J. Alloys Compd. 857, 157554 (2021); https://doi.org/10.1016/j.jallcom.2020.157554
[8] Q.Q. Xiong, J.J. Lou, X.J. Teng, X.X. Lu, S.Y. Liu, H.Z. Chi, Z.G. Ji, J. Alloys Compd. 743, 377 (2018); https://doi.org/10.1016/j.jallcom.2018.01.350
[9] H. Liu, D. Su, G. Wang, S.Z. Qiao, J. Mater. Chem. 22(34), 17437 (2012); https://doi.org/10.1039/c2jm33992g
[10] X. Xu, X. Li, J. Zhang, K. Qiao, D. Han, S. Wei, W. Xing, Z. Yan, Electrochim. Acta 302, 259

824

(2019); https://doi.org/10.1016/j.electacta.2019.02.042

[11] S. H. Choi, Y. C. Kang, Nanoscale 7, 3965 (2015); https://doi.org/10.1039/C4NR06880G

[12] Y. Wang, D. Kong, S. Huang, Y. Shi, M. Ding, Y.V. Lim, T. Xu, F. Chen, X. Li, H.Y. Yang, J. Mater. Chem. A 6, 10813 (2018); https://doi.org/10.1039/C8TA02773K

[13] J. P. Huang, D. D. Yuan, H. Z. Zhang, Y. L. Cao, G. R. Li, H. X. Yang, X. P. Gao, Rsc Advances 3(31), 12593 (2013); https://doi.org/10.1039/c3ra42413h

[14] Y. Wang, D. Kong, W. Shi, B. Liu, G.J. Sim, Q. Ge, H.Y. Yang, Adv. Energy Mater. 6(21), 1601057 (2016); https://doi.org/10.1002/aenm.201601057

[15] G. Jia, H. Wang, D. Chao, H. He, N.H. Tiep, Y. Zhang, Z. Zhang, H.J. Fan, Nanotechnology 28(42), 42LT01 (2017); https://doi.org/10.1088/1361-6528/aa8c55

[16] B. Qu, C. Ma, G. Ji, C. Xu, J. Xu, Y.S. Meng, T. Wang, J.Y. Lee, Adv. Mater. 26(23), 3854 (2014); https://doi.org/10.1002/adma.201306314

[17] X. Li, J. Zai, Y. Liu, X. He, S. Xiang, Z. Ma, X. Qian, J. Power Sources 325,675 (2016); https://doi.org/10.1016/j.jpowsour.2016.06.090

[18] S. Huang, Q. He, W. Chen, Q. Qiao, J. Zai, X. Qian, Chem. Eur. J. 21(10), 4085 (2015); https://doi.org/10.1002/chem.201406124

[19] X. Rui, Z. Lu, H. Yu, D. Yang, H.H. Hng, T.M. Lim, Q. Yan, Nanoscale 5, 556 (2013); https://doi.org/10.1039/C2NR33422D

[20] J. Liu, P.J. Lu, S. Liang, J. Liu, W. Wang, M. Lei, S. Tang, Q. Yang, Nano Energy 12, 709 (2015); https://doi.org/10.1016/j.nanoen.2014.12.019

[21] S. Huang, Q. He, W. Chen, Q. Qiao, J. Zai, X. Qian, Chemistry 21(10), 4085 (2015); https://doi.org/10.1002/chem.201406124

[22] X. Li, J. Zai, Y. Liu, X. He, S. Xiang, Z. Ma, X. Qian, J. Power Sources 325, 675 (2016); https://doi.org/10.1016/j.jpowsour.2016.06.090

[23] M.C. Liu, H. Zhang, Y.X. Hu, C. Lu, J. Li, Y.G. Xu, L.B. Kong, Sustain. Energy Fuels 3, 1239 (2019); https://doi.org/10.1039/C9SE00047J

[24] X. Li, J. Zhang, Z. Liu, K. Qiao, D. Han, S. Wei, W. Xing, Z. Yan, J. Alloys Compd. 766, 656 (2018); https://doi.org/10.1016/j.jallcom.2018.07.008

[25] Y. Liu, N. Zhang, H. Kang, M. Shang, L. Jiao, J. Chen, Chem. Eur. J. 21(33), 11878 (2015); https://doi.org/10.1002/chem.201501759

[26] Q. Pang, Y. Gao, Y. Zhao, Y. Ju, H. Qiu, Y. Wei, B. Liu, B. Zou, F. Du, G. Chen, Chem. Eur. J. 23(19),7074 (2017); https://doi.org/10.1002/chem.201700542

[27] H. Wang, Q. Yuan, D. Wang, G. Chen, X. Cheng, T. Kups, P. Schaaf, Sustain. Energy Fuels 3, 865 (2019); https://doi.org/10.1039/C8SE00566D

[28] Y.V. Lim, Y. Wang, L. Guo, J.I. Wong, L.K. Ang, H.Y. Yang, J. Mater. Chem. A 5, 10406 (2017); https://doi.org/10.1039/C7TA01821E

[29] X. Zhang, W. Lei, X. Ye, C. Wang, B. Lin, H. Tang, C. Li, Mater. Lett. 159, 399 (2015); https://doi.org/10.1016/j.matlet.2015.07.044

[30] X. H. Zhang, Z. Wang, H. Tan, M. Q. Xue, Chalcogenide Lett. 18(11), 735 (2021).